

# Nanostructured gas sensors and electrical characterization of deposited SnO<sub>2</sub> nanoparticles in ambient gas atmosphere

T.P. Hülser<sup>a,b,\*</sup>, H. Wiggers<sup>b</sup>, F.E. Kruis<sup>c</sup>, A. Lorke<sup>a</sup>

<sup>a</sup> Faculty of Science, Institute of Physics, AG Lorke, Campus Duisburg, University Duisburg-Essen, 47057 Duisburg, Germany

<sup>b</sup> Institute of Combustion and Gas Dynamics, Campus Duisburg, University of Duisburg-Essen, Germany

<sup>c</sup> Process and Aerosol Measurement Technology, University of Duisburg-Essen, Campus Duisburg, 47057 Duisburg, Germany

Available online 25 April 2005

## Abstract

SnO<sub>2</sub> nanoparticles with small particle size distribution ( $\sigma < 1.2$ ), and diameters of 10, 15 and 20 nm are deposited on platinum interdigital transducers with 2  $\mu\text{m}$  finger width and 2  $\mu\text{m}$  spacing. Impedance spectroscopy measurements in synthetic air, taken in the temperature range between 100 and 250 °C show a clear dependence of the measured impedance on the particle size. Three different contributions to the overall impedance have been resolved for 10 nm particles and assigned to the contribution of bulk, intergranular contact and electrode contact. Particles of larger diameters do not allow such a clear distinction. The experimental observations have been analyzed by fitting the measured data with equivalent circuit functions, where typical serial connections of simple  $R$  and parallel  $RC$ s are used for fitting. As expected for a semiconducting material, the resistance decreases with increasing temperature. Activation energies of the different charge carrier transport processes were determined from Arrhenius plots.

© 2005 Elsevier B.V. All rights reserved.

**Keywords:** SnO<sub>2</sub>; Tin oxide; Nanoparticles; Gas sensing; Impedance spectroscopy; Activation energy

## 1. Introduction

Within the past decades, solid state sensors based on SnO<sub>2</sub> have become an important analytical devices for air monitoring in domestic and industrial environment [1]. Most of the commercially available sensors are produced by ceramic fabrication technologies or by thick film technology with SnO<sub>2</sub> pastes as the starting material [2,3]. Nevertheless these sensors exhibit several disadvantages, such as poor selectivity, long response and stabilizing times and high power consumption [1,4], which can be overcome by modern thin film technologies. Especially the utilization of nanosized powders in thin film technologies is of increasing interest due to the high surface to volume ratio and their large surface area [5].

It is well known that the resistance of metal oxide semiconductors can be affected by temperature as well as by ambient gases [5,6]. Since the interaction of these materials with gaseous medium depends on their structure and surface, impedance spectroscopy is a useful tool for a detail characterization [7]. Coupled with additional physical characterization, impedance spectroscopy can yield a specific insight into the various occurring phenomena, within the device. The most important advantage of such ac measurements is that they can distinguish individual contributions to electrical conduction and polarizing effects arising from different sources like grain and bulk boundaries, intergranular contact and grain/electrode contact, whereas dc measurements show only the overall effect of all contributions [8]. However, the method suffers from the disadvantage that only integral information across the whole sample area can be obtained. Especially in the case of polydisperse particulate materials, a broadening and smearing of the obtained impedance spectra is observed.

\* Corresponding author.

E-mail addresses: [huelser@vug.uni-duisburg.de](mailto:huelser@vug.uni-duisburg.de) (T.P. Hülser), [wiggers@uni-duisburg.de](mailto:wiggers@uni-duisburg.de) (H. Wiggers), [e.kruis@uni-duisburg.de](mailto:e.kruis@uni-duisburg.de) (F.E. Kruis).

The current paper focuses on the investigation of SnO<sub>2</sub> thin films fabricated from size-selected nanoparticles ( $\sigma \leq 1.2$ ) in the size regime between 10 and 20 nm.

## 2. Experimental

### 2.1. Sample preparation

The device fabrication is described in detail by Kennedy et al. [9]. SnO was evaporated as precursor material for the synthesis of SnO<sub>x</sub> nanoparticles, which offers significant advantages over Sn or SnO<sub>2</sub>. As substrate, interdigitated structures having an active area of 1 mm<sup>2</sup> are used. For this purpose, a method was developed for a localized deposition. An electrostatic precipitator was modified into a low-pressure impactor by adding a nozzle (with an inner diameter between 0.5 and 2 mm and positioned 2 mm above the substrate) and evacuating the deposition chamber down to 3 mbar. The inertial focusing of the nanoparticle aerosol results in a deposition spot as small as 200 μm when using the 0.5 mm nozzle, so that films with a thickness above 100 nm can be formed rapidly. The particles exhibit a small size distribution, with a geometric standard deviation of  $\sigma < 1.2$  as described in [9].

### 2.2. Sensor geometry

The structure with interdigitated electrodes was developed in cooperation with the Fraunhofer Institute, IMS, Duisburg, Germany. In order to enable electrical measurements of the deposited, highly resistive SnO<sub>x</sub> nanoparticles, a 1 mm<sup>2</sup> structure consisting of 160 interdigitated fingers with a width and a separation of 2 μm was fabricated on a chip 3 mm × 3 mm in size. The electrodes are buried in phosphor-

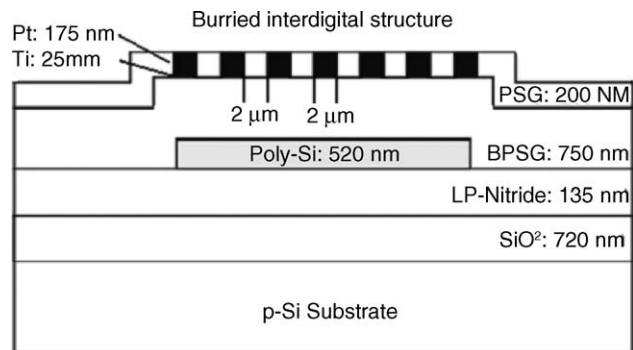


Fig. 1. Schematic draw of the sensor design.

doped silicate glass (PSG), which has a high resistance and suitable viscous behaviour during processing. A schematic of the structure is shown in Fig. 1. The resistance of the structure without deposited film is more than 1 GΩ. The structures are bonded to a DIL8 chip carrier.

### 2.3. Measurement setup

For the impedance measurements, a Solatron SI 1255 frequency response analyzer (FRA) in combination with a dielectric interface SI 1296 was used in the frequency range between 1 Hz and 1 MHz. Fig. 2 shows a schematic draw of the applied setup.

The sample was kept in a gas-tight chamber, filled with a gas inlet and outlet and connected to a gas mixing system and a vacuum pump (Fig. 2). A temperature-controlled tube furnace was used to heat the chamber to a given temperature between 100 and 250 °C.

Before measuring the impedance of different materials, the following procedure was applied to all samples. First the

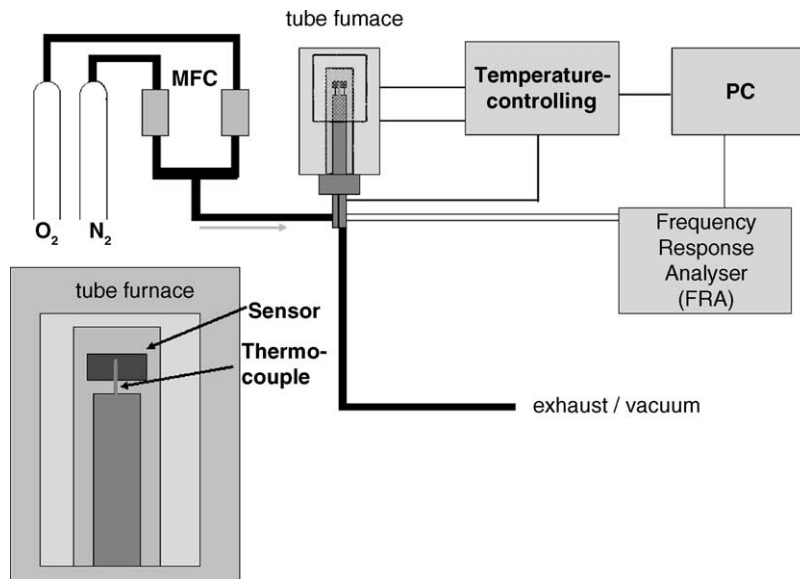


Fig. 2. Schematic draw of the experimental setup. The inset in left bottom shows a magnification of the tube furnace.

samples were dried and stabilized by heating at 300 °C in vacuum ( $10^{-5}$  mbar) for several hours. Afterwards, the vacuum line was closed and dry synthetic air (80% N<sub>2</sub>, 20% O<sub>2</sub>) was blown through the chamber at atmospheric pressure for some additional hours. Then the chamber was cooled to 100 °C and the ac-impedance measurements were carried out in the temperature range between 100 and 250 °C in steps of 10 °C (with 17 measurement points/decade in frequency). Before starting an impedance measurement, the system was thermally stabilized for 30 min at the desired temperature. The temperature deviation during the measurements was less than  $\pm 0.3$  °C.

### 3. Results and discussion

The impedance data for particles with a particle size of 20, 15 and 10 nm have been measured in the temperature range from 100 to 250 °C. Fig. 3a shows the Bode plot of the impedance measurements on 20 nm sized particles for 180 and 200 °C. The decrease of resistance with increasing temperature is a well-known property of semiconducting materials. All measurements on this particle size exhibit an almost ideal semicircle. This can be ascribed to a very narrow relaxation time distribution due to the fact that the sensor material consists of nearly monodisperse SnO<sub>2</sub> particles and it indicates that the electron scattering processes are homogeneous.

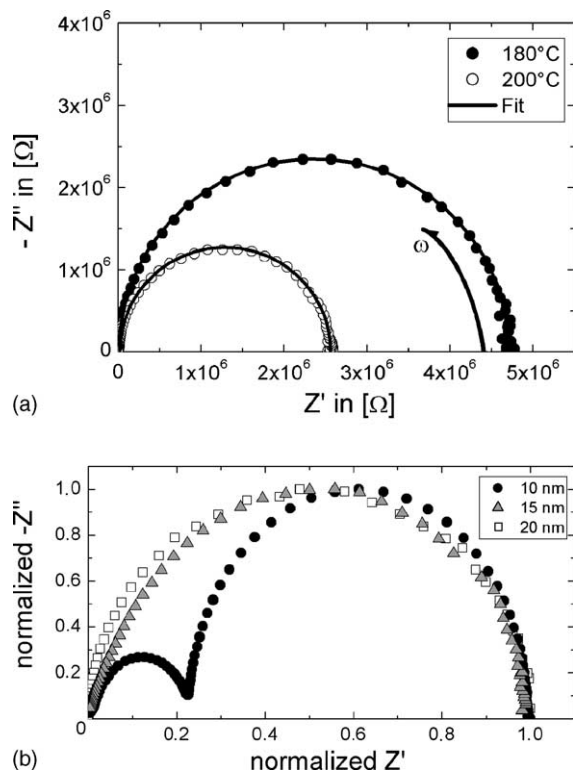


Fig. 3. (a) Impedance data in Bode representation for 20 nm particles and the lines of best fit. The inset shows a magnification of the high frequency range. (b) Normalized impedance data in Bode representation for 10 nm/15 nm/20 nm particles at 150 °C.

For the investigation of size-dependent properties in the charge carrier processes, additional sensors with 15 and 10 nm have been examined. The preparation of the materials and the measuring procedure were the same as described above. For a direct comparison of the measurements, Fig. 3b displays the normalized Bode plots of all samples. As can be seen from the diagram, a transition in the impedance data takes place. While the 20 nm particles show one relaxation process, a slight shoulder at higher frequencies is observable in the case of 15 nm particles whereas the 10 nm particles show two well-separated semicircles. The small semicircle as well as the shoulder can be distinguished by plotting the imaginary part of the modulus  $M''$  versus the measuring frequency using

$$M'' = \omega C_0 Z' \quad (1)$$

with the angular velocity  $\omega = 2\pi f$  and the background capacity  $C_0$  of the platinum chip arrangement. Fig. 4 shows the normalized imaginary part of the modulus for the three samples. In the case of 20 nm particles, only one signal at about  $10^4$  Hz can be observed. Its maximum corresponds to the maximum of the semicircle in the Bode representation. The spectrum of the 15 nm particles as well as the spectrum of the 10 nm particles exhibit two signals that are only slightly separated in the case of 15 nm particles but well separated in the case of 10 nm particles. The shoulder at  $10^3$  Hz corresponds to the large low-frequency semicircle in the Bode plot, while the big signal at  $10^6$  Hz corresponds to the small high-frequency semicircle.

The overall electrical conductivity of SnO<sub>2</sub> particles is dependent on the concentration of oxidizing and reducing agents in the surrounding atmosphere. In the presence of oxygen, its chemisorption on the particles leads to a depletion of charge carriers within the surface layer, whereas in the presence of reducing agents the desorption of oxygen increases the charge carrier concentration [10,11]. The depletion of charge carriers due to the chemisorption of oxygen has been explained by pulling electrons out of the tin oxide particle

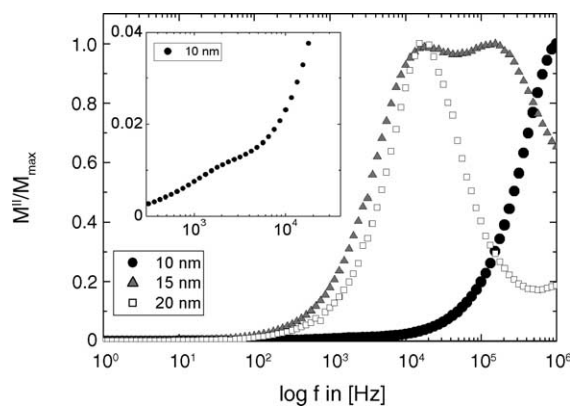


Fig. 4. Normalized imaginary part of the modulus function against frequency for 10, 15 and 20 nm sized particles. The inset shows the magnification of the spectrum for 10 nm particles in a frequency range from  $3 \times 10^2$  to  $4 \times 10^4$  Hz.

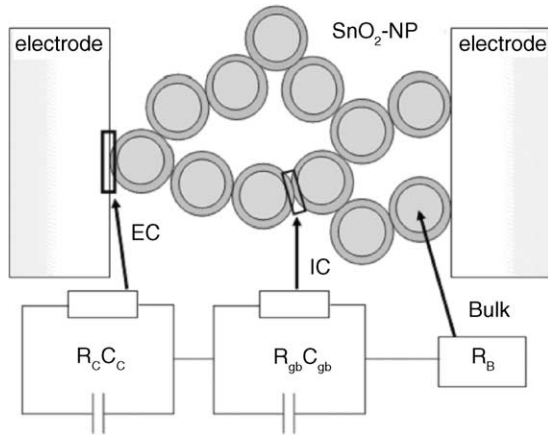


Fig. 5. Schematic draw of the charge carrier processes in  $\text{SnO}_2$  sensor systems and according equivalent circuit diagram.  $R_c C_c$  describes the electrode/particle contact,  $R_{gb} C_{gb}$  matches with the intergranular contact and  $R_B$  is the bulk resistance of the core.

surface [12]. The  $\text{SnO}_2$  ( $\text{SnO}_x$ ) core of the particles is assumed to be unaffected and a well conducting core remains.

Due to their size, this sensing effect is more dominant in the case of nanosized particles than in micrometer sized particles. Barsan and Weimar describe a model for the charge carrier transport within a particulate  $\text{SnO}_2$  sensor [13]. They postulate three different contributions to the overall conduction mechanism: intergranular contact, bulk conductivity and electrode contact. From this model, an equivalent circuit was developed. It consists of  $R_B$  representing the bulk contribution, a parallel ( $R_{gb} C_{gb}$ ) element for the intergranular contact, and a parallel ( $R_c C_c$ ) element for the electrode contact. Fig. 5 shows the adapted equivalent circuit diagram and a schematic drawing of the charge carrier transport processes. The capacitive contribution of the electrode contact (EC) originates from the capacitance between the electrode and the conducting core, surrounded by a less conducting  $\text{SnO}_2$  shell. For the same reason the intergranular contact (IC) also requires a parallel RC unit.

For a quantitative analysis of our measurements, the data obtained within the temperature range between 100 and  $250^\circ\text{C}$  have been fitted using the adequate equivalent circuit. Due to the fact that in the case of 20 nm particles only one relaxation process has been observed, the equivalent circuit was reduced by one RC-element, otherwise the problem would have been over-determined.

The agreement between measurement and fit is very good ( $R=0.99$ ) as can be seen from the drawn lines in Fig. 3a and Fig. 6. (Note that not only the position and diameter of each semicircle is fitted, but that every measured point in the complex plane is accurately reproduced.) The fit results of the different resistances have been used to calculate the activation energies  $E_a$  of the different conduction processes using equation:

$$G = G_0 e^{-E_a/k_b T} \quad (2)$$

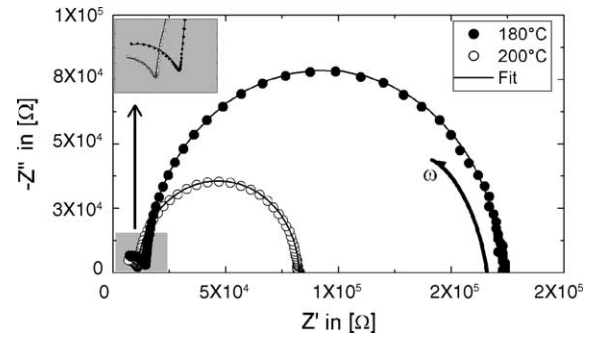
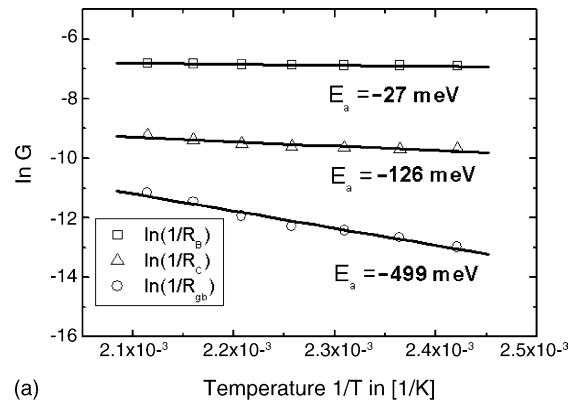
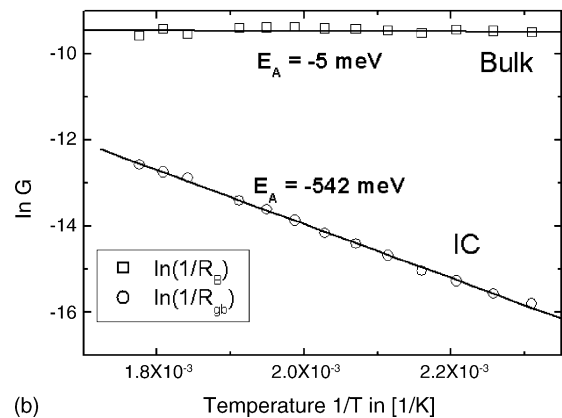


Fig. 6. Impedance data in Bode representation for 10 nm particles and the lines of best fit. The inset shows a magnification of the high frequency range.

Fig. 7a and b shows the Arrhenius plots of the conductivities  $G=1/R$  calculated from the fit on 10 and 20 nm particles. The smallest activation energy has been assigned to the bulk contribution ( $R_B$ ) and exhibits values of the same order of magnitude for both particle sizes. Probably due to a size effect, the activation energy for the 20 nm particles with a bigger, well conducting core is lower. Likewise, the highest activation energy which is assigned to the intergranular



(a)



(b)

Fig. 7. (a) Arrhenius diagrams of the different charge carrier transport processes for 10 nm particles. The activation energies  $E_a$  calculated from the slope are given in the plot. (b) Arrhenius diagrams of the different charge carrier transport processes for 20 nm particles. The activation energies  $E_a$  calculated from the slope are given in the plot.

contact is smaller for particles with 10 nm in size (−499 meV) compared to the 20 nm particles (−542 meV). The analysis of the remaining electrode-particle contribution (EC) results in an activation energy of −126 meV. The assignments of EC and IC bases on the simple model that the distance of two conducting particle cores is bigger than the distance between one core, surrounded by the SnO<sub>2</sub> shell, and the electrode.

The fact that the impedance measurements of the small, monodisperse SnO<sub>2</sub> particles show such structured spectra allows a much closer insight to the sensing mechanism of SnO<sub>2</sub>. It opens the opportunity to distinguish between sensing mechanisms that need the interface electrode/SnO<sub>2</sub>/gas phase and sensing mechanisms that influence the core/shell structure directly. With this knowledge, multisensing devices with only one particle size may be operated by simply switching the measuring frequency.

#### 4. Outlook

First steps have been made to produce sensors in nanometer dimensions with small finger distances. To distinguish systematically between the contribution of the intergranular contact (IC) and the electrode contact, structures with different finger widths and finger distances will be produced.

#### 5. Conclusion

SnO<sub>2</sub> particles were deposited on platinum interdigital structures to realize gas sensitive sensors. Impedance measurements of these SnO<sub>2</sub> thin films were taken in an oxygen/nitrogen atmosphere. The nanoparticles sensors exhibit different behaviour, which directly depend on their particle size. Different frequency dependent contributions to the overall resistance for 10, 15 and 20 nm particles have been detected. The different contributions were separated using equivalent circuit diagrams. Due to the fact that the measurements have been performed on nearly monodisperse particles, the contributions of the bulk, the electrode contact and the intergranular contact could be well separated. From Arrhenius plots, the activation energies of the different conduction processes have been determined.

#### Acknowledgements

Thanks to M.K. Kennedy and H. Fissan for contributing the sensors. Financial support of the Deutsche Forschungsgemeinschaft (SFB 445) is gratefully acknowledged.

#### References

[1] Y. Shimizu, E.D. Bartolomeo, E. Traversa, G. Gusmano, T. Hyodo, K. Wada, M. Egashira, Effect of surface modification on No. 2 sensing properties of SnO<sub>2</sub> varistor-type sensors, *Sens. Actuators B* 60 (1999) 118–124.

[2] G. Martinelli, M.C. Carotta, Thick-film gas sensors, *Sens. Actuators B* 23 (1995) 157–161.

[3] M. Prudenziati, Thick-film technology, *Sens. Actuators A: Phys.* 25 (1–3) (1990) 227–234.

[4] K. Ihokura, J. Watson, *The Stannic Oxide Gas sensor: Principles and Applications*, CRC press, Boca Raton, FL., 1994.

[5] N.S. Baik, G. Sakai, K. Shimanoe, N. Miura, N. Yamazoe, Hydrothermal treatment of tin oxide sol solution for preparation of thin-film sensor with enhanced thermal stability and gas sensitivity, *Sens. Actuators B* 65 (2000) 97–100.

[6] A. Dieguez, A. Romano-Rodriguez, J.R. Morante, J. Kappler, N. Barsan, W. Göpel, Nanoparticle engineering for gas sensor optimisation: improved sol–gel fabricated nanocrystalline SnO<sub>2</sub> thick film gas sensor for NO<sub>2</sub> detection by calcination, catalytic metal introduction and grinding treatments, *Sens. Actuators B* 60 (1999) 125–137.

[7] E. Endres, H.D. Jander, W. Göttler, A test system for gas sensors, *Sens. Actuators B* 23 (1995) 163–172.

[8] O.K. Varghese, L.K. Malhotra, Studies of ambient dependent electrical behaviour of nanocrystalline SnO<sub>2</sub> thin films using impedance spectroscopy, *J. Appl. Phys.* 87 (2000) 7457–7465.

[9] M. Kennedy, F.E. Kruis, H. Fissan, B.R. Metha, S. Stappert, G. Dumpich, Tailored nanoparticle films from monosized tin oxide nanocrystals: particle synthesis, film formation, and size-dependent gas-sensing properties, *J. Appl. Phys.* 93 (2003) 551.

[10] H. Ogawa, M. Nishikawa, A. Abe, Hall measurement studies and an electrical conduction model of tin oxide ultrafine particle films, *J. Appl. Phys.* 53 (1982) 4448–4455.

[11] J.M. Herrmann, J. Disdier, A. Fernandez, V.M. Jimenez, J.C. Sanchez-Lopez, Oxygen gas sensing behavior of nanocrystalline tin oxide prepared by the gas phase condensation method, *Nanostruct. Mater.* 8 (1997) 675–686.

[12] S.C. Chang, Oxygen chemisorption on tin oxide: correlation between electrical conductivity and EPR measurements, *J. Vac. Sci. Technol. B* 17 (1980) 366–369.

[13] N. Barsan, U. Weimar, Understanding the fundamental principles of metal oxide based gas sensors; the example of CO sensing with SnO<sub>2</sub> sensors in the presence of humidity, *J. Phys.: Condens. Mater.* 15 (2003) 813–839.

#### Biographies

**Tim Patrick Huelser** is graduated with a degree in Physics at the Gerhard-Mercator-University Duisburg, Germany. He is currently working on his PhD thesis in the experimental physics department of the University of Duisburg-Essen. His research focuses on the magnetic and electrical properties of metallic and semi-conducting nanoparticles.

**Hartmut Wiggers** received his PhD degree in inorganic chemistry from the University of Essen in 1993. During his postgraduate research he was involved with the characterization of charge carrier transport processes in semi-conducting and quantum-sized materials with AC and DC methods. His work also focussed on the electrical characterization of sensors based on microporous host/guest compounds. Since 1998 he is employed as a senior research scientist at the nanomaterials group of the Institute of Combustion and Gas Dynamics, University of Duisburg. His current research interests are the formation, chemistry and physics of crystalline, nanosized inorganic materials, particularly oxidic and non-oxidic semi-conductors.

**Frank Einar Kruis** received a PhD at the TU Delft, Netherlands, working on particle synthesis. He was EU research fellow at the “Laboratoire des Sciences du Génie Chimique”, Nancy, France and investigated turbulent mixing processes. In 2001 he obtained the lecture qualification with the topic “Synthesis of nanoparticles in the gas phase for functional applications”. He is now working at the Institute for Process and Aerosol Measurement Technology, University of Duisburg-Essen, Germany.

**Axel Lorke** is a professor of experimental physics at University Duisburg-Essen, Germany since 2000. He received his PhD from the Ludwig-Maximilian University Munich in 1991 for his work on GaAs/AlGaAs superlattices. Thereafter, he joined the Materials Department at the University of California, Santa Barbara, where he worked on self-assembled

quantum dots. His work in Duisburg focuses on the electronic and optical properties of self-assembled quantum-dots, electronic transport in symmetry-broken systems, and spectroscopy of nanoparticles formed in the gas-phase.